Journal of Physics D: Applied Physics

Time-resolved characterization of plasma properties in a CH_4/He nanosecond-pulsed dielectric barrier discharge

To cite this article before publication: Timothy Y. Chen *et al* 2019 *J. Phys. D: Appl. Phys.* in press https://doi.org/10.1088/1361-6463/ab0598

IOP Publishing Journal Title
Journal **XX** (XXXX) XXXXXX https://doi.org/XXXX/XXXX

Time-resolved Characterization of Plasma Properties in a CH_4/He Nanosecond-pulsed Dielectric Barrier Discharge

Timothy Y. Chen[1], Aric C. Rousso[1], Shuqun Wu [1,2], Benjamin M. Goldberg[1], H J van der Meiden[3], Yiguang Ju[1], and Egemen Kolemen[1,4]

[1] Department of Mechanical and Aerospace Engineering, Princeton University, Princeton, USA
[2] Center for More Electric Aircraft Power System, College of Automation Engineering, Nanjing University of Aeronautics and Astronautics, Nanjing, Jiangsu 210016, China
[3] FOM Institute DIFFER- Dutch Institute For Fundamental Energy Research, Trilateral Euregio Cluster, Associate EURATOM-FOM, BL-3430 BE Nieuwegein, The Netherlands
[4] Princeton Plasma Physics Laboratory, Princeton, USA

E-mail:

Abstract

Non-equilibrium plasmas for plasma-assisted combustion, pollutant remediation, fuel reforming, and catalysis rely on the production of energetic electrons that ionize, dissociate, and excite the fuel and oxidizer molecules. Experimental characterization of the electron temperature, electron density, and vibrational temperature are necessary to validate and improve plasma kinetic models. An experimental apparatus capable of Thomson scattering and vibrational Raman scattering measurements in the same discharge with molecular admixtures was developed. Both diagnostics are necessary to study the induced vibrational non-equilibrium from electron impact. Thomson scattering spectra were resolved by placing a physical mask at the output of a single grating spectrometer. The electron temperature and density and the impact of hydrocarbon addition was measured for a 60 Torr CH_4/He nanosecond pulsed plane-to-plane dielectric barrier discharge with 0% to 2% CH_4 addition. Electron densities as low as 1 x 10^{12} cm^{-3} and electron temperatures ranging from 0.5 eV to 9 eV were observed. A decrease in the electron temperature and density was observed even with 1% CH_4 addition. Moreover, the addition of N_2 to the discharge enabled vibrational Raman scattering and quantification of the first level vibrational temperature starting from 75 ns after the voltage pulse. The electron temperature and density were also measured in this CH_4/N_2/He mixture by Thomson scattering. Addition of N_2 led to a faster electron temperature decay than in the original CH_4/He mixture. The advantages and disadvantages of this detection scheme for Thomson scattering over the triple grating spectrometer and the volume Bragg grating notch filter is discussed.

Keywords: Thomson scattering, vibrational Raman scattering, non-equilibrium plasma, plasma-assisted fuel reforming

1. Introduction

Low temperature non-equilibrium plasmas have been investigated for applications in plasma-assisted combustion **[1], [2]**, fuel reforming and pollutant control **[3]**, and catalysis **[4]**. Furthermore, there is significant interest in reforming CH_4, a strong greenhouse gas, to H_2 **[5]**, syngas **[6]**, and higher hydrocarbon liquid fuels and chemicals **[4], [7]** by low temperature plasmas. These plasmas enable fuel conversion and chemical synthesis close to room temperature due to dissociative reactions via collisions with highly energetic electrons.

For plasma-assisted combustion and fuel reforming, electron-impact reactions play a major role in creating radicals and excited species that enhance oxidation. Lefkowitz et al. found that 24% of the methane consumption was attributed to dissociative electron impact reactions, while 53% was attributed to reactions with $O(^1D)$, an excited oxygen atom produced through electron impact with oxygen molecules **[8]**. Snoeckx et al. found that in a CH_4/CO_2 plasma the top three reactions for consuming both the fuel and oxidizer were dissociative electron impact reactions **[9]**. The branching ratios of these reactions and the subsequent chemistry depends on the non-Boltzmann electron energy distribution function (EEDF) and the electron number density. Therefore, time-resolved measurements of electron temperature and number density are crucial for validation of plasma chemistry models and further understanding of the underlying kinetics.

However, to our knowledge, electron temperature and density of nanosecond-pulsed discharges have only been measured in noble gases with planar metal electrodes **[10]**, noble gas mixtures with diatomic molecules in a tip-to-tip filament plasma **[11], [12]**, and in atmospheric air also using a tip-to-tip geometry **[13], [14]**. Few measurements have been conducted in a uniform volumetric nanosecond-pulsed plane-to-plane dielectric barrier discharge (ns-DBD) involving fuels. Since hydrocarbons like CH_4 have more vibrational degrees of freedom that can be excited by a broad electron temperature range, the electron energy distribution function may evolve differently from that of a H_2 containing plasma. Also, since ions in a methane discharge have faster recombination rates **[15]**, the electron density could be different from a pure He discharge even with small amounts of CH_4 addition. It is worth noting that Narishige et al. have reported Thomson scattering measurements in a H_2/CH_4 microwave plasma **[16]**. Unfortunately, these measurements were not time-resolved.

Furthermore, the degree of vibrational non-equilibrium induced by the plasma is of interest as both a model validation target and a pathway toward efficient chemical conversion through "vibrational ladder climbing" **[17]** and lowering the effective reaction activation energy as predicted by the Fridman-Macheret $\boldsymbol{\alpha}$ model **[18]**. Vibrational temperature of nanosecond-pulsed plasmas in N_2 and O_2 mixtures has been extensively measured **[19]–[24]**. However, few measurements of the vibrational temperature has been made in a discharge containing CH_4. Combined vibrational temperature and electron property measurements would provide key validation targets for predicting the electron energy transfer in plasma kinetic models.

In this study, using a newly developed setup, Thomson scattering will be used to measure time-resolved bulk electron temperature and electron density in plane to plane He and CH_4/He ns-DBD. For the first time, both vibrational Raman scattering and Thomson scattering will be used to characterize the non-equilibrium dynamics in a CH_4/N_2/He ns-DBD.

2. Experimental Setup

We introduce a new experimental setup for studying plasma chemistry named Plasma Enhanced Chemistry eXperiment (PECX). The experimental apparatus consists of three parts: the laser entrance optics, the plane to plane ns-DBD cell, and the detection optics. Figure 1 shows the entire experimental setup for Thomson and Raman scattering.

Incoherent Thomson scattering, where the laser wavelength is shorter than the Debye length, is typically employed as an *in situ* diagnostic for measuring the electron temperature and density in low temperature plasmas. Thomson scattering requires elimination of stray light at the laser wavelength due to Rayleigh scattering and reflections. This is usually done with either a triple grating spectrometer **[10], [25]–[27]** or a volume Bragg grating notch filter **[28], [29]** for systems utilizing a frequency doubled Nd:YAG laser. Both of these options require extensive alignment and cost associated with the optics. In this letter, we introduce a simple setup using a single spectrometer paired with a physical mask to deal with the stray light. This approach can be thought of as a triple grating spectrometer setup without the second and third gratings and has been implemented at Magnum-PSI for low pressure discharges **[30]**. This work extends this detection strategy to moderate pressures and electron densities of 10^{12} cm^{-3}. In this study, the smallest Debye length was approximately $5\boldsymbol{\mu m}$ resulting in a Salpeter parameter $\boldsymbol{\alpha}$ of 0.01, so the scattering was in the incoherent regime.

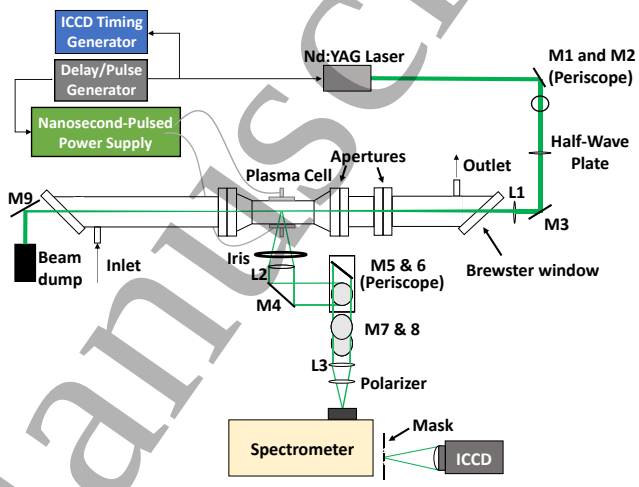

Figure 1. PECX setup for Thomson and Raman scattering in a plane-to-plane ns-DBD. L and M are used to denote lenses and mirrors, respectively.

In addition, removing the polarizer and mask while adding a longpass filter allows for vibrational Raman scattering measurements. Due to the small Raman cross-section of the $\boldsymbol{\nu_2}$ and $\boldsymbol{\nu_4}$ modes of CH_4 and the complexity of modeling the $\boldsymbol{\nu_1}$ and $\boldsymbol{\nu_3}$ bands **[31], [32]**, vibrational Raman scattering is performed through the addition of N_2. This technique is well established, making validation of the setup possible. Both Raman and Thomson scattering will be performed in a CH_4/N_2/He mixture.

2.1 Laser Entrance Optics

A Quantel Q-Smart 850 Nd:YAG laser was used to generate a 6 ns full width at half maximum (FWHM) laser pulse with a pulse energy of 230 mJ. The pulse energy was measured at the laser output before each run with an energy meter (Ophir PE50BF-DIF-C). The shot-to-shot variation in pulse energy during each measurement was estimated to be ±5%. The laser beam was directed into the chamber using a periscope and a half-wave plate to ensure vertical polarization entering the chamber, due to the periscope's rotation of the laser polarization. An f=1300 mm AR-coated plano-convex lens was used to focus the beam to the discharge region. Brewster windows at the entrance and exit of the chamber were used to reduce stray light. Before the discharge region,

"subcritical" and "critical" apertures were placed to ensure that stray light does not enter the collection optics as in **[30]**. The critical aperture was 6 mm in diameter and was located 365 mm away from the center of the discharge. The subcritical aperture was 12 mm in diameter and was located 110 mm from the discharge.

2.2 Dielectric Barrier Discharge Cell

The plasma was generated using 44.5 mm by 44.5 mm electrodes with a gap distance of 14 mm, similar to those used in [8], [33], [34]. The nanosecond pulses were generated by a FID GmBH FPG 30-50MC4 power supply capable of delivering 12 ns FWHM and 32 kV peak applied voltage pulses at 30 kHz. Both positive and negative pulses were used in this study, totalling 9 kV. The total applied voltage pulse, current, and coupled energy are shown in Figure 2. Similar to **[35]**, the coupled energy was calculated by cumulatively integrating the electrical power from the applied voltage and current. The asymptotic value is the final coupled energy. The voltage and current were aligned in time such that the coupled energy was minimized to zero for the case of no discharge while voltage was applied. Furthermore, this "open-load" condition was used to subtract any interfering noise in the current signal from the power supply. Helium (Airgas 99.999% purity), Nitrogen (99.998% purity) and Methane (Airgas 99.5% purity) cylinders were used in these experiments. The gases were delivered using MKS GE50A mass flow controllers, and the pressure was set by an MKS 946 PID controller connected to an MKS 153D throttle valve and a Baratron 626C manometer. The voltage pulse and the laser pulse were monitored using a Tektronix P6015A voltage probe and Thorlabs DET10A2 photodiode. The current was measured using a Pearson 6585 current monitor.

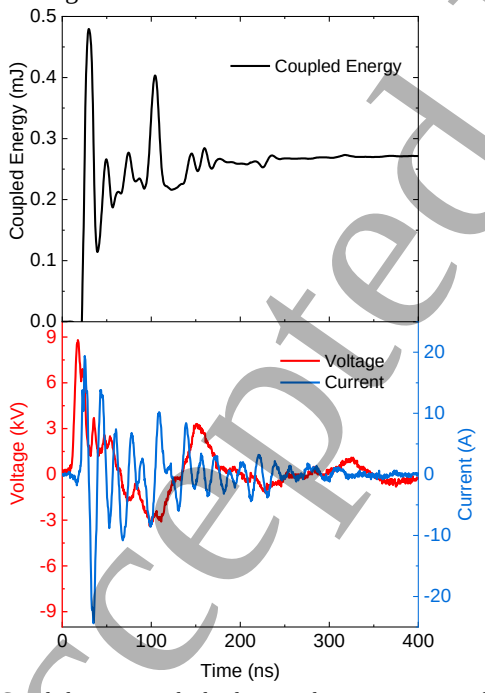

Figure 2. Coupled energy, applied voltage, and current over a single pulse.

2.3 Detection Optics

The scattered light was collected and focused by two f = 150 mm 1-inch AR-coated achromatic lenses. A board with black felt was placed behind the cell to serve as a viewing dump. All mirrors in the detection branch are 2 inch diameter to reduce possible vignetting. Since the lens is smaller than the mirrors, a 2 inch iris is placed in front of the lens to limit the amount of stray light that can pass around the lens. Also, an enclosure made of black hardboard isolates the collection optics from stray reflections. A film polarizer was placed in front of the slit to enable accurate calibration by rotational Raman scattering. The spectrometer (Acton 2500i, f = 0.500 m, 2400 gr/mm holographic VIS optimized) then disperses the light into a spectrum. A slit width of 150 $\boldsymbol{\mu m}$ was used for Thomson scattering measurements, and a slit width of 250 $\boldsymbol{\mu m}$ was used for the vibrational Raman scattering measurements. For vibrational Raman scattering measurements, the polarizer was replaced with a longpass filter to ensure minimal levels of stray light.

At the focal plane of the spectrometer output, a blackened aluminum mask was aligned to block the stray light. The mask was mounted on two 1-axis micrometer translation stages for precise alignment in the wavelength and focal axes. The mask enabled many on-chip charge-coupled device (CCD) accumulations which improves the signal to noise ratio of the measurement. Vertical pixels on the intensified CCD (ICCD) camera were hardware binned so that only a single row of pixels contributed read noise. Any residual light that leaked through the mask was subtracted out by a background measurement. Two mask widths were used. A 2 mm wide mask which blocks a 0.6 nm half-width was used for the pure helium discharge, while a 2.8 mm mask which blocks a 0.9 nm half-width was used for the CH_4/He and CH_4/N_2/He mixtures. A thinner mask was able to be used in the pure helium discharge due to the smaller Rayleigh scattering cross-section of helium compared to methane.

After passing through the mask, the light is focused by a camera lens (NIKKOR 50 mm 1.4/g) reverse mounted with a reversing ring (Fotodiox RB2A 58mm). The lens was reverse mounted so that the image magnification on the CCD chip was close to one. With this arrangement, only a single camera lens was needed to relay the image from the mask to the ICCD (Princeton Instruments PIMAX 1300, UNIGEN II intensifier). 20 ns gate widths were used to account for any time jitter.

3. Calibration and Data Processing

3.1 Relative and Absolute Calibrations

Relative calibration of the instrument's response to different wavelengths was performed with a Tungsten lamp (StellarNet SL1-CAL) following a similar procedure as **[36]** . Since the Tungsten lamp is a blackbody emitter, comparison of the recorded spectra and a blackbody emission curve gives the instrument response function. Using this response, every measured spectrum can be corrected for the various transmission curves of the optical components such as the ICCD camera and the diffraction grating. Furthermore, the response of the detection branch to polarized and depolarized

light was determined by measuring the Tungsten spectra with a polarizer parallel and perpendicular to the laser polarization.

Thomson spectra were absolutely calibrated by rotational Raman scattering of N_2 at 60 Torr. The measured rotational Raman spectrum was fitted with a code based on **[37]** with a fixed rotational temperature of 300 K. Further details about rotational Raman calibration of Thomson scattering are available in **[25], [27], [28]**.The ratio of the area under the J = 6 →8 Stokes Raman transition and the area under the Thomson spectrum was used to calculate the absolute electron number density through the following relation:

$$\frac{A_{TS}}{A_{Raman}} = \frac{\left(\frac{d\sigma_{N_2\,J=6\to8}}{d\Omega} * n_{N_2 J=6}\right)}{\left(\frac{d\sigma_{TS}}{d\Omega} * n_e\right)} \qquad (1)$$

where A_{TS} and A_{Raman} are the integrated Thomson and Raman spectra with respect to wavelength, $\frac{d\sigma_{N_2\,J=6\to8}}{d\Omega}$ is the differential cross section for the N_2 J=6 to 8 Raman transition, $\frac{d\sigma_{TS}}{d\Omega}$ is the Thomson scattering differential cross section, $n_{N_2 J=6}$ is the number density of N_2 in the J=6 rotational energy level, and n_e is the electron number density. Taking the ratio of the two areas eliminates system-specific parameters like transmission efficiency from the scattering equation. The density of N_2 in the J=6 rotational level and the Raman differential cross section were calculated from the fit and assumes a Boltzmann distribution for the rotational energy levels. The instrumental broadening for the Raman peaks was fitted to an experimental He Rayleigh scattering spectrum by using a Gaussian lineshape. A rotational Raman spectrum is measured before and after every Thomson measurement and averaged to account for any drifts in the laser energy. To eliminate Rayleigh scattering from the rotational Raman spectrum, the depolarized Raman spectrum was used. A depolarization ratio of 3/4 was assumed, and the Raman spectrum was rescaled by the ratio of the polarized and depolarized Tungsten spectra.

3.2 Data Processing

The Thomson spectrum was extracted through background subtraction of a measurement 400 ns before the voltage pulse. In the case of strong plasma emission, a spectrum with the plasma on without the laser and a dark current spectrum were measured to subtract the emission. The resultant spectrum was assumed to be Maxwellian and fitted with a Gaussian profile while excluding the data points blocked by the mask. Significant deviations from a Gaussian line shape were not observed for the data presented in this letter. Following Carbone et al **[38]**, if the plot of the natural logarithm of the Thomson scattering spectrum versus the electron energy is linear, then the EEDF can be represented as Maxwellian. Figure 3 shows the logarithm of the Thomson scattering intensity at 15 ns in the 0% CH_4 case, a best fit Maxwellian EEDF, and a best fit Druyvesteyn EEDF **[39]**, **[40]**. Due to insufficient sensitivity and wavelength range, deviations from a Maxwellian EEDF could be present at higher electron energies but cannot be observed with this experimental apparatus. Therefore, the measurements presented are the bulk electron density and temperature. Examples of the Thomson and rotational Raman fits are shown in Figure 4.

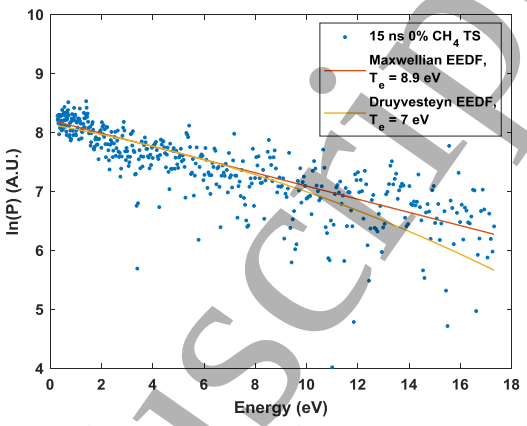

Figure 3. Plot of the natural logarithm of the Thomson spectrum at 15 ns in 0% CH_4, a Maxwellian EEDF, and a Druyvesteyn EEDF.

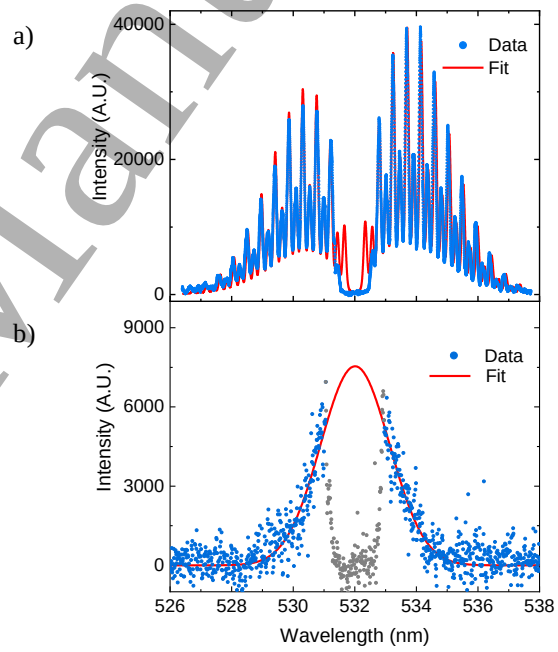

Figure 4. (a) Calibration N_2 rotational Raman scattering. (b) Thomson scattering Spectrum in 1% CH_4/He mixture, taken 100 ns after the pulse.

Electron temperatures are evaluated from the 1/e half-width of the fitted Gaussian profile using the following expression **[25]**:

$$T_e = \frac{m_e c^2}{8k_B \sin^2\theta/2}\left(\frac{\Delta\lambda_{1/e}}{\lambda_0}\right)^2 \qquad (2)$$

The electron number densities are calculated by rearranging (1) to the following form:

$$n_e = \frac{\left(A_{Raman} * \frac{d\sigma_{N_2\,J=6\to8}}{d\Omega} * n_{N_2 J=6}\right)}{\left(A_{TS} * \frac{d\sigma_{TS}}{d\Omega}\right)} \qquad (3)$$

Vibrational Raman scattering spectra are fitted using the following skew-normal distribution:

$$f = I \exp\left(-\left(\frac{\lambda - \lambda_0}{\omega}\right)^2\right)\left(1 + \mathrm{erf}\left(\alpha(\lambda - \lambda_0)\right)\right) \qquad (4)$$

where I is an intensity factor, ω is a scale parameter, λ_0 is the peak position, and α is a skewness factor. The areas of the ground state peak (v=0) and first vibrational level peak were integrated to find the first level vibrational temperature defined below:

$$T_{v01} = \frac{\theta_{vib}}{\ln\left(\frac{A_0}{A_1}\right)} \qquad (5)$$

where θ_{vib} is the characteristic vibrational temperature of N_2, A_0 is the area under the ground state peak, and A_1 is the area under the first vibrational level peak. The first level peak intensity was divided by 2, according to the v+1 scaling of the Raman cross-section for harmonic oscillators **[22]**.

4. Results and Discussion

4.1 Electron Density and Temperature in CH_4/He

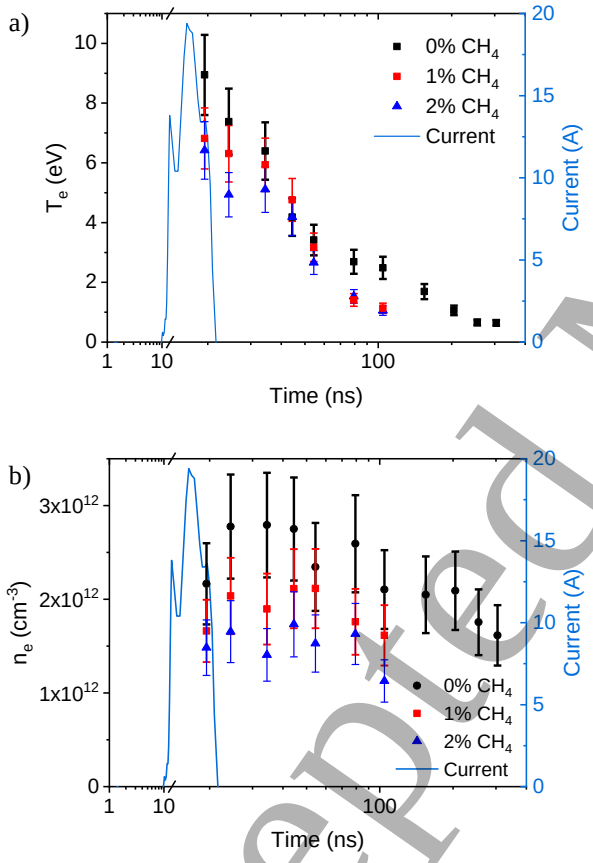

Figure 5. Time-resolved (a) electron temperature and (b) density with varying CH_4 addition. The discharge current is shown as a reference. 0 ns on the time axis refers to the start of the voltage pulse.

Time-dependent electron temperature and density measurements were made in a CH_4/He plasma for varying CH_4 concentrations as shown in Figure 5. Depending on the required signal to noise ratio, 2,000 to 5,000 laser shots were on-chip accumulated and 5 to 6 spectra were averaged per data point. The uncertainties in electron temperature and density were 15% and 20%, respectively. This uncertainty was based on the fitting confidence intervals and also the uncertainty in the Raman cross-section for calibrating the electron density. The voltage pulses were repeated at 100 Hz, with the positive half plotted alongside the electron temperature and density for reference. The pressure was kept at 60 Torr with an overall flow speed of 1.26 m/s. Note that this means that the cell was not fully flushed out between each plasma pulse. Around half of the scattered photons came from gas that had two pulses applied and the other half had three pulses applied. However, the interpulse time was 10 ms, so variations between pulses from electron accumulation was assumed to be negligible.

From Figure 5a, the electron temperature decreased faster with CH_4 addition compared to the pure Helium discharge. More than 0.8 eV of temperature difference was observed between any two datasets within the first 30 ns. Since CH_4 has additional energy transfer pathways such as vibrational excitation and dissociation, then a lower electron temperature would be expected as electron energy is directed through those channels. Later in the afterglow for the CH_4/He plasmas, the final electron temperature was approximately the same. This suggests that as the electron temperature decreases, the evolution of the electron temperature was no longer significantly influenced by collisions with CH_4 molecules. This could be due to superelastic collisions with He metastables as discussed by Roettgen et al. **[11]**.

Figure 5b shows that as more CH_4 was introduced into the discharge, the overall electron number density decreased. However, the slopes of the decay curves in the afterglow did not change significantly with the addition of CH_4. This suggests that faster electron-ion recombination was not the primary contribution to the difference between the three decay curves. Instead, the difference can be explained through the drop in electron temperature discussed previously. As electron energy is transferred to dissociation and vibrational excitation of CH_4 molecules, the electron temperature and the overall available energy for ionization decreases. Thus, the overall electron density would decrease.

4.2 Combined Electron Density, Electron Temperature, and Vibrational Temperature Measurements in CH_4/N_2/He

The vibrational non-equilibrium was measured by replacing 5% of the He content with N_2 in the 2% CH_4/He mixture. Since the plasma properties could not be guaranteed to be the same as without N_2 addition, Thomson scattering was performed as well. The nanosecond pulser was operated in a burst of 100 pulses at 30 kHz using the same voltage setting as the CH_4/He datasets. However, due to the specificities of the pulser, the same applied voltage setting produced a 10 kV pulse in the burst mode instead of a 9 kV pulse. Therefore, the comparisons with the CH_4/He measurements are only qualitative. The burst of pulses was introduced to ensure that

the vibrational temperature above the detection limit. The signal-to-noise ratio of the v=1 peak limits the detectable vibrational temperature to approximately 1000 K. The burst repetition rate was 10 Hz, and the flow speed was 0.5 m/s which ensured that the discharge region was flushed between bursts. Thomson scattering measurements were carried out for the first 100 ns after the 100th pulse, while the vibrational Raman scattering was measured starting from 75 ns after the 100th voltage pulse. The vibrational temperature was not measured before 75 ns due to signal to noise limitations. Furthermore, the uncertainty in the electron temperature and density increased as compared to the CH_4/He measurements due to significant plasma emission from electronically excited N_2. 2500 on-chip accumulations were used per Thomson scattering spectrum and 8 spectra were averaged per data point. 3000 to 3500 on-chip accumulations were used for the vibrational Raman scattering, and 4 to 5 spectra were averaged per data point. The uncertainty in the Thomson scattering measurements was calculated based on the fitting errors, which was at most 25% for the electron temperature and 50% for the electron density. The uncertainty of the vibrational Raman scattering measurement was estimated to be 15%, since the Lorentzian wings of the peaks could not be fully captured by the skewed Gaussian lineshape.

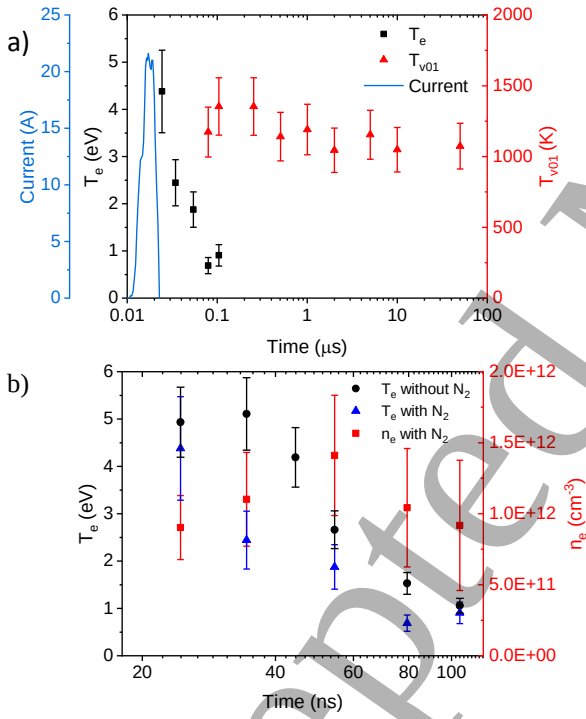

Figure 6. (a) Vibrational temperature and electron temperature of a CH_4/N_2/He discharge after the 100th voltage pulse. (b) Electron density and temperature for the first 100 ns of the discharge. 0 ns on the time axis refers to the start of the voltage pulse.

From Figure 6a, the vibrational temperature increases to ~1350 K after the electron temperature drops below 1 eV, and decreases to 1100 K after 50 μs. The vibrational-translational (V-T) relaxation time of N_2 can be up to 100 μs in low temperature discharges **[1]**. This long V-T relaxation time allowed for vibrationally excited N_2 populations to build up during the 33 μs inter-pulse time. The magnitude of the vibrational temperature is close to the temperature measured in a 10 kHz 100 Torr air ns- DBD experiment by Montello et al., and a similar slow decay in the vibrational temperature was observed **[19]**.

Comparing Figure 6b with Figure 5, the addition of N_2 dropped the electron temperature by more than 1 eV during the first 50 ns and the electron density on average dropped also. Furthermore, the electron temperature dropped to 1 eV faster than in the CH_4/He mixture. This could be because the electron-impact cross sections for vibrational excitation of N_2 peak for electron energies around 1-3 eV **[41]**, so electrons would cool faster in this energy range. Additionally, some amount of electron energy went into electronic excitation, as emission from the first positive system of N_2 was observed in the Raman measurements. This would explain the somewhat lower electron temperature early in the afterglow. Future work includes validating and using a 0-D kinetic model **[42]** to explain these trends in detail.

4.3 Laser Perturbations of the Plasma

To verify that laser perturbations such as He_2 Rydberg molecule photoionization **[12]** did not cause substantial errors in electron number density or temperature, the laser pulse energy was varied from 20 mJ to 50 mJ for Thomson scattering measurements in 60 Torr of pure He. The pulse repetition rate was a continuous 1 kHz with a residence time of approximately 80 ms, which applied 80 pulses to the discharge. In this arrangement, perturbations from build-up of any long-lived plasma-produced species would be detectable. Therefore, using a 1 kHz frequency is more prone to perturbations than those in the 100 Hz case, and as will be discussed below, no such perturbations were observed. Also, since 80 pulses have been applied, it makes it unlikely that perturbations due to build up of plasma-produced species exist in the 30 kHz 100-pulse burst measurement. All spectra were taken 150 ns after the voltage pulse and used 21,600 to 54,000 total laser shots per spectrum.

As seen in Figure 7 the extracted electron density was constant within the error bars for all pulse energies. Furthermore, laser heating via inverse bremsstralung did not affect the electron temperature within the uncertainty of the measurement. As the pulse energy gets lower, the uncertainty increases due to the weaker scattering signal at lower laser intensities. The influence of photoionized He_2^{Ry} molecules is also shown to not be large. The formation of these Rydberg molecules is through the following 3-body reactions **[43]**:

$$He^{**} + He + He \rightarrow He_2^{Ry} + He \quad (6)$$

$$He_2^{+} + He + e^{-} \rightarrow He_2^{Ry} + He \quad (7)$$

Both (6) and (7) depend on pressure and electron number density to produces He_2^{Ry} molecules. Since the discharge is at 60 Torr and the electron density is ~10^{12} cm^{-3}, both of these reaction channels would not be expected to produce significant amounts of Rydberg molecules.

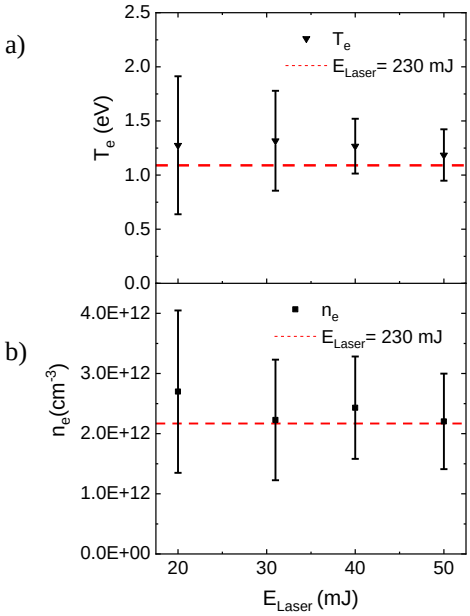

Figure 7. Electron temperature (a) and density (b) for varying laser pulse energies in a pure He discharge. The dashed line corresponds to the temperature or density extracted for a laser pulse energy of 230 mJ.

To evaluate the influence of ponderomotive forces on the electron density, we use equation 8 from **[44]**. Inputting $n_{e,0}$ = 10^{12} cm^{-3}, T_e = 0.5 eV, and $r_L \approx$ 10 $\boldsymbol{\mu}$m calculated from a Gaussian beam assumption, and I_0 = 4.9 x 10^{15} W/m^2 calculated from a pulse energy of 230 mJ, the perturbation is calculated to be 0.01%.

4.4 Advantages and disadvantages of the physical mask

Finally, the advantages and limitations of the this stray light elimination scheme are discussed. As mentioned previously, this method was implemented at Magnum-PSI for low pressure discharges **[30]**. A similar approach was used by van de Sande **[25]** and Brehmer et al. **[45]** where a strip of paper was placed immediately in front of the ICCD. Placing the mask at the focal plane of the spectrometer allows for more precise alignment, since the position can be adjusted via micrometer-driven translation stages. Furthermore, the mask can be machined to a specific width, depending on the amount of stray light encountered in the discharge. This makes this setup flexible in the types of mixtures that can be measured. Compared to a triple grating spectrometer, the current setup has the advantage of increased transmission efficiency since fewer optics are used. Furthermore, a single grating spectrometer is all that is required, which reduces the setup complexity. A volume Bragg grating notch filter is superior in terms of stray light rejection, but the alignment requirements are strict. As noted by Klarenaar et al. **[46]**, the notch filter has an acceptance angle of less than 0.1°, so the scattered light must be well-collimated. The main limitation of the physical mask is that large amounts stray light may prevent enough on-chip CCD accumulations to resolve the Thomson scattering signal. Therefore, this approach is well-suited for low to moderate pressure discharges. Measurements in high pressure discharges will require electron densities larger than those encountered in this work.

5. Conclusions

We introduced a new experimental apparatus, PECX, for study of coupled plasma properties and chemistry. This setup was demonstrated to be capable of time-dependent measurements for both Thomson and vibrational Raman scattering in the same discharge using a single spectrometer. Furthermore, it does not require a volume Bragg grating notch filter or three gratings, making Thomson scattering a more accessible technique for low to moderate pressure discharges. Electron number density and temperature were measured in a 60 Torr CH_4/He nanosecond-pulsed dielectric barrier discharge with CH_4 concentrations varying between 0% and 2%. Electron densities as low as 1 x 10^{12} cm^{-3} and electron temperatures from 0.5 to 9 eV were measured. The results showed that even addition of a few percent of CH_4 to the discharge caused a distinct decrease in the electron number density and temperature. Combined measurements of vibrational temperature, electron temperature, and electron density were performed in a CH_4/N_2/He discharge. Addition of N_2 also qualitatively decreased the electron density and temperature as compared to the 2% CH_4/He discharge. The decrease in electron number density was most likely not because of faster electron-ion recombination but rather due to the overall decrease of the electron temperature from the additional molecular energy modes available for energy transfer by electrons. The vibrational temperature was shown to rise rapidly during the discharge and early afterglow period to 1350 K via electron impact excitation and decrease slowly to around 1100 K after 50 $\boldsymbol{\mu s}$. The overall magnitude of the vibrational temperature corresponds well with a similar ps-CARS measurement **[19]**, thereby validating the Raman diagnostic. The present data provided valuable experimental targets to develop validated plasma kinetic models. Future work will include utilizing this setup for validation of plasma kinetic models, adding species measurements through Raman scattering and laser absorption, and exploring methods to overcome the small Raman cross-section for the $\boldsymbol{\nu_2}$ mode of CH_4 such as adding another laser pass like in **[21]**. By doing so, a more complete understanding of plasma-assisted combustion and fuel reforming will be realized.

Acknowledgements

This work was supported by ExxonMobil through its membership in the Princeton E-filliates Partnership of the Andlinger Center for Energy and the Environment. ACR and YJ are partially supported by the DOE-NETL-UCFER and ONR plasma research grants. TYC is partially supported through the Program in Plasma Science and Technology at Princeton University Fellowship.

References

[1] A. Starikovskiy and N. Aleksandrov, "Plasma-assisted ignition and combustion," *Progress in Energy and Combustion Science*, vol. 39, no. 1, pp. 61–110, Feb. 2013.

[2] Y. Ju and W. Sun, "Plasma assisted combustion: Dynamics and chemistry," *Progress in Energy and Combustion Science*, vol. 48, pp. 21–83, Jun. 2015.

[3] W. Wang, R. Snoeckx, X. Zhang, M. S. Cha, and A. Bogaerts, "Modeling Plasma-based CO_2 and CH_4 Conversion in Mixtures with N_2, O_2, and H_2O: The Bigger Plasma Chemistry Picture," *The Journal of Physical Chemistry C*, vol. 122, no. 16, pp. 8704–8723, Apr. 2018.

[4] L. Wang, Y. Yi, C. Wu, H. Guo, and X. Tu, "One-Step Reforming of CO_2 and CH_4 into High-Value Liquid Chemicals and Fuels at Room Temperature by Plasma-Driven Catalysis," *Angewandte Chemie International Edition*, vol. 56, no. 44, pp. 13679–13683, Oct. 2017.

[5] O. Khalifeh, A. Mosallanejad, H. Taghvaei, M. R. Rahimpour, and A. Shariati, "Decomposition of methane to hydrogen using nanosecond pulsed plasma reactor with different active volumes, voltages and frequencies," *Applied Energy*, vol. 169, pp. 585–596, May 2016.

[6] M. Scapinello, L. M. Martini, G. Dilecce, and P. Tosi, "Conversion of CH_4 /CO_2 by a nanosecond repetitively pulsed discharge," *Journal of Physics D: Applied Physics*, vol. 49, no. 7, p. 075602, Feb. 2016.

[7] A. Indarto, "A review of direct methane conversion to methanol by dielectric barrier discharge," *IEEE Transactions on Dielectrics and Electrical Insulation*, vol. 15, no. 4, pp. 1038–1043, Aug. 2008.

[8] J. K. Lefkowitz, P. Guo, A. Rousso, and Y. Ju, "Species and temperature measurements of methane oxidation in a nanosecond repetitively pulsed discharge," *Philosophical Transactions of the Royal Society A: Mathematical, Physical and Engineering Sciences*, vol. 373, no. 2048, p. 20140333, Aug. 2015.

[9] R. Snoeckx, R. Aerts, X. Tu, and A. Bogaerts, "Plasma-Based Dry Reforming: A Computational Study Ranging from the Nanoseconds to Seconds Time Scale," *The Journal of Physical Chemistry C*, vol. 117, no. 10, pp. 4957–4970, Mar. 2013.

[10] C.-G. Schregel, E. A. D. Carbone, D. Luggenhölscher, and U. Czarnetzki, "Ignition and afterglow dynamics of a high pressure nanosecond pulsed helium micro-discharge: I. Electron, Rydberg molecules and He (2^3S) densities," *Plasma Sources Science and Technology*, vol. 25, no. 5, p. 054003, Sep. 2016.

[11] A. Roettgen, I. Shkurenkov, M. Simeni Simeni, I. V. Adamovich, and W. R. Lempert, "Time-resolved electron temperature and electron density measurements in a nanosecond pulse filament discharge in H_2–He and O_2–He mixtures," *Plasma Sources Science and Technology*, vol. 25, no. 5, p. 055008, Aug. 2016.

[12] A. Roettgen, I. Shkurenkov, M. Simeni Simeni, V. Petrishchev, I. V. Adamovich, and W. R. Lempert, "Time-resolved electron density and electron temperature measurements in nanosecond pulse discharges in helium," *Plasma Sources Science and Technology*, vol. 25, no. 5, p. 055009, Aug. 2016.

[13] D. Z. Pai, G. D. Stancu, D. A. Lacoste, and C. O. Laux, "Nanosecond repetitively pulsed discharges in air at atmospheric pressure—the glow regime," *Plasma Sources Science and Technology*, vol. 18, no. 4, p. 045030, Nov. 2009.

[14] D. Z. Pai, D. A. Lacoste, and C. O. Laux, "Nanosecond repetitively pulsed discharges in air at atmospheric pressure—the spark regime," *Plasma Sources Science and Technology*, vol. 19, no. 6, p. 065015, Dec. 2010.

[15] E. M. Anokhin, M. A. Popov, I. V. Kochetov, A. Yu Starikovskiy, and N. L. Aleksandrov, "Kinetic mechanism of plasma recombination in methane, ethane and propane after high-voltage nanosecond discharge," *Plasma Sources Science and Technology*, vol. 25, no. 4, p. 044006, Aug. 2016.

[16] S. Narishige *et al.*, "Thomson Scattering Diagnostics of Glow Discharge Plasmas Produced in Raman Active Gases," *Japanese Journal of Applied Physics*, vol. 41, no. Part 2, No. 11A, pp. L1259–L1262, Nov. 2002.

[17] T. Kozák and A. Bogaerts, "Splitting of CO_2 by vibrational excitation in non-equilibrium plasmas: a reaction kinetics model," *Plasma Sources Science and Technology*, vol. 23, no. 4, p. 045004, Jun. 2014.

[18] A. Fridman, *Plasma Chemistry*. Cambridge, UK: Cambridge University Press, 2008.

[19] A. Montello, Z. Yin, D. Burnette, I. V. Adamovich, and W. R. Lempert, "Picosecond CARS measurements of nitrogen vibrational loading and rotational/translational temperature in non-equilibrium discharges," *Journal of Physics D: Applied Physics*, vol. 46, no. 46, p. 464002, Nov. 2013.

[20] A. Roettgen, W. Lempert, and I. Adamovich, "Measurements of N_2 Vibrational Distribution Function in Pulsed Nanosecond Nonequilibrium Discharge by Spontaneous Raman Scattering," in *51st AIAA Aerospace Sciences Meeting including the New Horizons Forum and Aerospace Exposition*, Grapevine (Dallas/Ft. Worth Region), Texas, 2013.

[21] A. Lo, G. Cléon, P. Vervisch, and A. Cessou, "Spontaneous Raman scattering: a useful tool for investigating the afterglow of nanosecond scale discharges in air," *Applied Physics B*, vol. 107, no. 1, pp. 229–242, Apr. 2012.

[22] W. R. Lempert and I. V. Adamovich, "Coherent anti-Stokes Raman scattering and spontaneous Raman scattering diagnostics of nonequilibrium plasmas and flows," *Journal of Physics D: Applied Physics*, vol. 47, no. 43, p. 433001, Oct. 2014.

[23] A. Lo, A. Cessou, and P. Vervisch, "Space and time analysis of the nanosecond scale discharges in atmospheric pressure air: II. Energy transfers during the post-discharge," *Journal of Physics D: Applied Physics*, vol. 47, no. 11, p. 115202, Mar. 2014.

[24] A. Lo, A. Cessou, P. Boubert, and P. Vervisch, "Space and time analysis of the nanosecond scale discharges in atmospheric pressure air: I. Gas temperature and vibrational distribution function of N_2 and O_2," *Journal of Physics D: Applied Physics*, vol. 47, no. 11, p. 115201, Mar. 2014.

[25] M. J. van de Sande, "Laser scattering on low temperature plasmas: high resolution and stray light rejection," Technische Universiteit Eindhoven, Eindhoven, The Netherlands, 2002.

[26] A. F. H. van Gessel, E. A. D. Carbone, P. J. Bruggeman, and J. J. A. M. van der Mullen, "Laser scattering on an atmospheric pressure plasma jet: disentangling Rayleigh, Raman and Thomson scattering," *Plasma Sources Science and Technology*, vol. 21, no. 1, p. 015003, Feb. 2012.

[27] E. Carbone and S. Nijdam, "Thomson scattering on non-equilibrium low density plasmas: principles, practice and challenges," *Plasma Physics and Controlled Fusion*, vol. 57, no. 1, p. 014026, Jan. 2015.

[28] B. Vincent, S. Tsikata, S. Mazouffre, T. Minea, and J. Fils, "A compact new incoherent Thomson scattering diagnostic for low-temperature plasma studies," *Plasma Sources Science and Technology*, vol. 27, no. 5, p. 055002, May 2018.

[29] B. L. M. Klarenaar, O. Guaitella, R. Engeln, and A. Sobota, "How dielectric, metallic and liquid targets influence the evolution of electron properties in a pulsed He jet measured by Thomson and Raman scattering," *Plasma Sources Science and Technology*, vol. 27, no. 8, p. 085004, Aug. 2018.

[30] H. J. van der Meiden *et al.*, "Advanced Thomson scattering system for high-flux linear plasma generator," *Review of Scientific Instruments*, vol. 83, no. 12, p. 123505, Dec. 2012.

[31] G. Magnotti, U. Kc, P. L. Varghese, and R. S. Barlow, "Raman spectra of methane, ethylene, ethane, dimethyl ether, formaldehyde and propane for combustion applications," *Journal of Quantitative Spectroscopy and Radiative Transfer*, vol. 163, pp. 80–101, Sep. 2015.

[32] E. Jourdanneau, F. Chaussard, R. Saint-Loup, T. Gabard, and H. Berger, "The methane Raman spectrum from 1200 to 5500cm−1: A first step toward temperature diagnostic using methane as a probe molecule in combustion systems," *Journal of Molecular Spectroscopy*, vol. 233, no. 2, pp. 219–230, Oct. 2005.

[33] A. Rousso, S. Yang, J. Lefkowitz, W. Sun, and Y. Ju, "Low temperature oxidation and pyrolysis of n-heptane in nanosecond-pulsed plasma discharges," *Proceedings of the Combustion Institute*, vol. 36, no. 3, pp. 4105–4112, 2017.

[34] A. Rousso, X. Mao, Q. Chen, and Y. Ju, "Kinetic studies and mechanism development of plasma assisted pentane combustion," *Proceedings of the Combustion Institute*, Jun. 2018.

[35] K. Takashima, Z. Yin, and I. V. Adamovich, "Measurements and kinetic modeling of energy coupling in volume and surface nanosecond pulse discharges," *Plasma Sources Science and Technology*, vol. 22, no. 1, p. 015013, Dec. 2012.

[36] C. J. Barth, C. C. Chu, M. N. A. Beurskens, and H. J. v. d. Meiden, "Calibration procedure and data processing for a TV Thomson scattering system," *Review of Scientific Instruments*, vol. 72, no. 9, pp. 3514–3527, Sep. 2001.

[37] B. L. M. Klarenaar, "Rotational temperature measurements in DBDs operating at atmospheric pressure," Technische Universiteit Eindhoven, Eindhoven, The Netherlands, 2014.

[38] E. A. D. Carbone *et al.*, "Experimental investigation of the electron energy distribution function (EEDF) by Thomson scattering and optical emission spectroscopy," *Journal of Physics D: Applied Physics*, vol. 45, no. 47, p. 475202, Nov. 2012.

[39] M. J. Druyvesteyn and F. M. Penning, "The Mechanism of Electrical Discharges in Gases of Low Pressure," *Reviews of Modern Physics*, vol. 12, no. 2, pp. 87–174, Apr. 1940.

[40] T. S. Brown and D. J. Rose, "Plasma Diagnostics using Lasers: Relations between Scattered Spectrum and Electron-Velocity Distribution," *Journal of Applied Physics*, vol. 37, no. 7, pp. 2709–2714, Jun. 1966.

[41] L. L. Alves, "The IST-LISBON database on LXCat," *Journal of Physics: Conference Series*, vol. 565, p. 012007, Dec. 2014.

[42] X. Mao, A. Rousso, Q. Chen, and Y. Ju, "Numerical modeling of ignition enhancement of CH 4 /O 2 /He mixtures using a hybrid repetitive nanosecond and DC discharge," *Proceedings of the Combustion Institute*, Jul. 2018.

[43] E. A. D. Carbone, C.-G. Schregel, and U. Czarnetzki, "Ignition and afterglow dynamics of a high pressure nanosecond pulsed helium micro-discharge: II. Rydberg molecules kinetics," *Plasma Sources Science and Technology*, vol. 25, no. 5, p. 054004, Sep. 2016.

[44] M. N. Shneider, "Ponderomotive perturbations of low density low-temperature plasma under laser Thomson scattering diagnostics," *Physics of Plasmas*, vol. 24, no. 10, p. 100701, Oct. 2017.

[45] F. Brehmer, S. Welzel, B. L. M. Klarenaar, H. J. van der Meiden, M. C. M. van de Sanden, and R. Engeln, "Gas temperature in transient CO_2 plasma measured by Raman scattering," *Journal of Physics D: Applied Physics*, vol. 48, no. 15, p. 155201, Apr. 2015.

[46] B. L. M. Klarenaar, F. Brehmer, S. Welzel, H. J. van der Meiden, M. C. M. van de Sanden, and R. Engeln, "Note: Rotational Raman scattering on CO_2 plasma using a volume Bragg grating as a notch filter," *Review of Scientific Instruments*, vol. 86, no. 4, p. 046106, Apr. 2015.